Conference on Modelling Fluid Flow (CMFF'22)
The 18th International Conference on Fluid Flow Technologies
Budapest, Hungary, August 30-September 2, 2022

A NOVEL MODEL FOR GLAZE ICE ACCRETION

Róbert-Zoltán SZÁSZ[1], Stefan IVANELL[2] and Johan REVSTEDT[3],

[1] Corresponding Author. Department of Energy Sciences, Lund University, PO.Box 118, SE-22100 Lund, Sweden. Tel.: +46 46 222 0480, E-mail: robert-zoltan.szasz@energy.lth.se
[2] Department of Earth Sciences, Uppsala University, Sweden, E-mail: stefan.ivanell@geo.uu.se
[3] Department of Energy Sciences, Lund University, Sweden, E-mail: johan.revstedt@energy.lth.se

ABSTRACT

This paper introduces a novel model to predict ice accretion in glaze ice conditions due to supercooled water droplets. Glaze icing is controlled by a large number of interacting physical phenomena. The purpose of the suggested model was to offer a faster alternative to explicitly modelling these phenomena. The paper presents the suggested model and investigates the sensitivity of the predictions on the model parameters for three experimental cases in the literature. The results indicate a qualitatively correct behaviour. Quantitatively, the model over-predicts the amount of accreted ice, the error being significantly larger in severe icing conditions. The errors are caused partly by the choice of faster numerical approaches and by the lack of possibility to account for detaching ice from the surface.

Keywords: CFD, glaze ice, ice accretion, LPT

NOMENCLATURE

A	$[m^2]$	area
dV_A	$[m^3]$	added ice volume
dV_T	$[m^3]$	ice volume to add
M	$[kg]$	mass
C	$[K/m]$	solution coefficient
LWC	$[kg/m^3]$	liquid water content
MVD	$[m]$	mean volumetric diameter
R	$[m]$	droplet radius
T	$[K]$	temperature
c_1	$[-]$	collision efficiency
c_2	$[-]$	sticking efficiency
c_3	$[-]$	accretion efficiency
e	$[-]$	impact elasticity coefficient
ft	$[s]$	freezing time
r	$[m]$	radius
t	$[s]$	time
$\underline{dx}$	$[m]$	displacement vector
$\underline{u}$	$[m/s]$	velocity
$\underline{x}$	$[m]$	position vector
α	$[^o]$	angle of attack
γ	$[m^2/s]$	thermal diffusivity
λ	$[1/m]$	solution coefficient
ω	$[-]$	under-relaxation factor
ϕ	$[kg/m^3]$	mass concentration of the particles
θ	$[K]$	temperature difference

Subscripts and Superscripts

N	normal
T	tangential
c	critical
e	exterior
i	initial
n	solution term index
rel	relative
k	iteration

1. INTRODUCTION

Wind power technology, as one of the tools to replace fossil fuels, gained a strong popularity during the past decades. Due to the rapid increase of the number and size of installed power plants, there are more and more wind turbines installed in less favourable areas, such as areas with cold climate conditions. It is estimated that about a quarter of the global installed wind energy capacity is located in areas prone to the risk of icing [1]. In some countries the share of wind turbines located in cold climate areas is significantly higher, e.g. in Sweden more than 80% of the installed capacity in 2020 was located in the most northerly quarter of the country [2].

Although cold climate areas have the advantage of generally lower population density (leading to better acceptance) and larger amount of extractable kinetic energy (for the same wind speed, due to the higher density), ice accretion imposes significant challenges for the manufacturers and for the wind turbine owners. The ice layer changes the aerodynamic shape of the blade, resulting in non-optimal profiles and a decrease of the extracted energy. Furthermore, the extra mass of the ice represents an extra load on the solid structures and may imbalance the

rotor causing vibrations which lead to earlier fatigue and, in extreme cases, mechanical failures. There is a safety hazard as well, ice chunks may detach from the blades and may travel relatively large distances. These chunks represent a danger for the persons or objects located in the turbines' neighbourhood. The current trend of increasing wind turbine sizes increases also the areas affected by ice throw.

The above-described challenges triggered research campaigns focusing on many aspects of ice accretion, like predicting weather conditions leading to ice accretion, investigating the accretion process itself, development of ice detection and de-icing devices, just to name a few research areas. A rather detailed overview of the related research is presented in [3].

The characteristics of the accreted ice depend on the prevailing meteorological conditions. Commonly, icing conditions are divided in two categories. In low temperature (usually below 10^oC) conditions, the water droplets are well below freezing temperature but are still in the liquid state. These supercooled droplets impacting on a surface freeze instantaneously upon contact, and begin to accrete forming rime ice, which is usually opaque due to the air trapped between the frozen droplets. For slightly higher temperatures, but still below freezing, (usually between 5 and 0^oC) the supercooled droplets do not freeze instantaneously upon contacting the surface. Instead, a water film is formed which may run along the surfaces before freezing, leading to the formation of a more compact, so-called glaze-ice. Of course, in practical situations a combination of rime and glaze conditions might occur as well.

The first studies of the impact of icing on airfoils date back to 1930's and originated in the aerospace community [4, 5]. Over the past two decades various authors presented more specific studies on the accretion on wind turbine blades. Makkonen [6, 7] was among the first ones to characterise different kind of icing events and to create models for it. Based on thermodynamic considerations the following model was proposed to predict the rate of ice accretion:

$$\frac{dM}{dt} = c_1 c_2 c_3 \phi \underline{u} A \tag{1}$$

where M is the mass of the ice, t the time, ϕ the mass concentration of particles, $\underline{u}$ the velocity of the particles relative to the object, A the cross sectional area of the object. c_1, c_2 and c_3 are correction factors having values between zero and one and account for the collision efficiency, sticking efficiency and accretion efficiency, respectively. For further details about the model the reader is referred e.g. to [7]. Eq. 1 is still the most widely used ice prediction model, often combined with other methods.

Usually, there is a scale separation between the flow field surrounding the blades and the rate of ice accretion on the blades. As a consequence, a common approach is to compute the ice accretion and the flow around the ice accreted airfoils in separate stages. For the flow computations a common approach is to use simplified methods to reduce the computational efforts. For example, a potential flow solver is used in LEWICE (although there is a possibility to import flow fields from other solvers) [8], whereas the panel method is used in TURBICE (see e.g. [9]). Recently, thanks to the increase in computational power and to the need to account for 3D effects, it is more and more common to solve the full set of Navier-Stokes equations (see e.g. [10, 11, 12]). Droplet transport is commonly modelled either in an Eulerian (e.g. [12]) or Lagrangian (e.g. [13, 14, 10]) framework.

In the case of rime ice conditions, since all droplets hitting the surface freeze instantaneously, there is no need for heat transfer computations. The amount of droplets hitting the surface is determined explicitly or specified via the collection efficiency, depending if a lagrangian or eulerian model is used for droplet transport. To model glaze ice, the most common approach is to compute 1D heat transfer problems based on the so-called Stefan's problem formulated for aeronautical applications by Messinger in 1953 and further improved by Myers in 2001 (see e.g. [10]). In [15] beside the heat transfer, the evolution of the water film formed on the blade surface is accounted as well.

Here, we propose an alternative approach to model glaze ice formation. Instead of accounting for all the interacting physical phenomena occurring during glaze ice formation (wall film formation, its evolution along the surface, heat transfer, etc.) we propose an extension of an already existing rime ice model.

Although its grounding in physics is limited, the suggested lower order model has the advantage of significantly lower complexity, leading to faster computing times. Beside presenting the model, the goal of the paper is to investigate the performance of the suggested model to predict light and severe glaze ice conditions.

2. METHODS

The aim of this work has been to provide a modelling approach which had to be integrated in a model chain where a large number of ice accretion cases had to be computed. For this reason the methods chosen herein are characterised by relatively high computational performance at the expense of somewhat limited accuracy.

The scale separation of the flow time scales and the time scales associated to the growth of the ice layer facilitates the use of staged computations: one determines the flow around the airfoil and then the amount of accreted ice. Nevertheless, in the case of severe icing conditions the ice structures formed on the surfaces may significantly change the flow topology. In order to account for such changes, a common approach is to divide the time interval of the

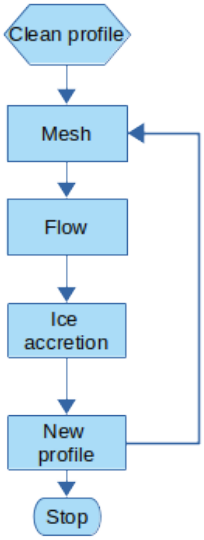

Figure 1. Steps of the multi-staged approach

entire icing event in sub-intervals. During each sub-interval the geometry is considered constant. Before the next time interval is computed, the surface (and the mesh used for the flow computations) is updated to account for the ice accreted during the previous interval. Such a multi-step approach is used e.g. in [10]. A sensitivity study to physical and modelling parameters affecting airfoil icing using such an approach is shown in [12].

Here, we use also such a multi-staged approach, the main steps being shown in Figure 1. The entire icing event will be computed in N_{st} steps. The number of steps is determined by the balance of desired accuracy and available computing time. Since the flow and the airfoil shape is assumed to not change during a step, a too low number of steps will result in decreased accuracy, especially in heavy icing conditions. At the other extreme, dividing the icing event into too many sub-intervals leads to very small changes in the airfoil shape, and therefore results in sub-optimal use of the computing resources.

The ice accretion simulations are performed using the open-source toolbox OpenFOAM [16] in combination with an in-house tool to adjust the airfoil surface based on the amount of ice accreted.

The computations start with the clean airfoil as input. In order to reduce the time needed for the computations only two-dimensional domains are considered. The mesh is generated in two stages. First the snappyHexMesh utility (included in OpenFOAM) is used to generate an unstructured 3D mesh around the airfoil. Next, the 2D mesh is obtained by extruding one of the sides of the 3D mesh.

For the purpose of improving the computational efficiency, the flow and ice accretion computations are separated. It is assumed that during a sub-stage the shape of the airfoil, and by this the flow, is not changing significantly. For this reason, the statistically stationary two-dimensional flow field is simulated first using the SST k-ω RANS model [17]. Thereafter, the ice accretion is determined by Lagrangian Particle Tracking (LPT) based on the steady flow field. The number of injected parcels and the injected droplets' diameter is determined to match the desired LWC. In the LPT computations only the particle drag force and the turbulent dispersion is accounted for. The turbulent dispersion is done with a stochastic model (a.k.a random walk).

Each parcel of Lagrangian particles that impacts the aerofoil surface is registered. Depending if rime- or glaze-ice conditions are computed, the droplet impacting the surface is considered to freeze immediately or is allowed to travel along the surface. The details of the glaze ice model are given in Section 3.

Once the amount and distribution of accreted ice is determined, the airfoil surface is updated using an in-house tool. Before updating the surface, two pre-processing stages are carried out.

First, the ice distribution is smoothed over the airfoil surface. This step is motivated by the fact, that even if the length of the LPT computations is long enough to achieve a statistically converged ice distribution, depending on the mesh resolution used to discretize the airfoil, there might be small cells with no ice accreted, leading to physically irregular shape of the ice accreted surface. This smoothing step is carried out by transferring the information of accreted ice in a mass-conservative manner from the cell centers to the mesh vortices and back. The effect of smoothing can be increased by increasing the number of smoothing loops.

The second pre-processing of the accreted ice mass aims to increase performance. Since the time scale of the flow and the ice accretion differ substantially, with the icing time scale being much longer, one can increase the computational efficiency by scaling the amount of accreted ice everywhere by a factor f, leading to a shortening of the time covered by the LPT computations with the same factor, f. The scaling is limited by the requirement of having statistically representative amount of ice accreted on the airfoil. Our previous investigations show that it is possible to decrease the time scale of ice accretion by a factor 1000, i.e., one second explicitly computed ice accretion can be scaled to predict accretion after 1000 s.

The new shape of the airfoil is determined by an iterative approach using an in-house tool. The tool reads in the surface mesh used in OpenFOAM to discretize the airfoil geometry and the amount of ice accreted on each mesh cell face. Based on the accreted ice mass and a user-provided density (which can be adjusted to account e.g. for trapped air) one can determine the added volume for each cell face and, by integrating it over all cells, the total ice volume to be added to the airfoil, dV_T. Based on the added volume, the face area and the face normal direction, one can compute an initial guess for the average dis-

placement vector at each node of the surface mesh, $\underline{dx}$, as the average of the displacement vectors needed for the surrounding cells. Based on the average displacement, the first approximation of the ice-accreted mesh shape can be obtained by $\underline{x}^1 = \underline{x}^0 + \omega * \underline{dx}$, where exponents 0 and 1 denote the old and new values, respectively, and ω is an under-relaxation factor (set to 0.8 in the present calculations). Based on the estimated positions of the surface nodes, the actually added ice volume, dV_A, can be determined. Since this volume usually differs from the target added volume, the positions of the surface mesh nodes are corrected iteratively using Equation 2, the stopping criterion being $|(dV_T - dV_A^k)/dV_T| < 10^{-10}$.

$$\underline{x}^{k+1} = \underline{x}^k + \omega * \underline{dx} * (dV_T - dV_A^k)/dV_T \tag{2}$$

Once the new airfoil shape is determined a new mesh is generated and the entire process is iterated until the total length of the icing event is covered.

3. GLAZE ICE MODEL

3.1. Goal

As mentioned earlier, in order to accurately model glaze ice conditions, one needs to use a multitude of interacting models to describe the impact of the droplets, the formation of the water film and the heat transfer between the air, the water film and the solid surfaces. The large number of required models renders the Computational Fluid Dynamics (CFD) computations heavy both directly, by increasing the computational time needed to evaluate the models, and indirectly due to slower convergence as a result of the large number of degrees of freedom. Furthermore, even if the individual models can be validated for certain conditions, when a large number of models are interacting the accuracy of the predictions may suffer.

Our goal was to develop a simpler and more efficient model to account for glaze conditions. The increased efficiency was planned to be achieved by reducing the number of physical phenomena explicitly accounted for which inherently leads to a reduced number of model parameters. As a drawback, the model is expected to be less general, requiring validation to adjust the model parameters.

3.2. Model description

The glaze model is an extension of the rime-ice model initially implemented in an in-house solver [13, 14] and later implemented in OpenFOAM as well. The main idea of the model is to not freeze instantaneously the parcels upon impact (as it is the case for rime ice), but let the droplets slide along the surface for a specified freezing time, ft. During this freezing period only the positions of the droplets are updated, the freezing conditions are not re-evaluated. Although this is a rather crude approximation, it is much more efficient than using e.g. a wall film model and heat transfer calculations.

Two options have been implemented for the time being: prescribed freezing time and a first order approximation.

3.2.1. Prescribed freezing time

This is the simplest model and, as the name suggests, requires that the user specifies the time delay, ft, until the droplets (modelling the wall film) freeze. Although very simplistic, this model adds very little computational effort, thus it is affordable to evaluate cases where rime-ice conditions can be evaluated. Although the accuracy is limited, one can easily carry out sensitivity studies and/or validation computations.

During validation computations, it was found that simply imposing a time delay is not sufficient to model glaze ice conditions, since the impacting droplets are deflecting from the surface. In reality the droplets more often attach to the wall due to surface tension effects. To account for this, an additional model parameter has been introduced, e, which can be used to adjust the elasticity of the impact, the normal component of the parcel velocity after impact being computed as $\underline{u}_\mathrm{N} = e \cdot \underline{u}_\mathrm{T}$, $\underline{u}_\mathrm{T}$ being the tangential component. Thus, the normal component can be zeroed by setting $e = 0$. Nevertheless, cancelling the normal component entirely is not physical either because, upon impact, the droplets are located in regions of the boundary layer with very low relative velocity and even long time delays lead to very small displacements of the parcels along the surface. In reality the droplets and the wall film have a non-zero thickness and experience larger relative velocities.

3.2.2. First order approximation

To avoid the need to directly impose the freezing time, a second possibility has been implemented. This approach is based on the heat transfer in a spherical droplet with uniform properties, initial temperature of T_i in a surrounding with the exterior temperature of T_e.

The governing equation in radial direction is:

$$\frac{1}{r^2}\frac{\partial}{\partial r}\left(r^2\frac{\partial \theta}{\partial r}\right) = \frac{1}{\gamma}\frac{\partial \theta}{\partial t} \tag{3}$$

where $\theta(r,t) = T - T_e$. The solution of Eq.3 is of the form:

$$\theta(r,t) = \sum_{n=1}^{\infty} \frac{C_n}{r} sin(\lambda_n r) exp(-\gamma \lambda_n^2 t) \tag{4}$$

The coefficients are given by:

$$C_n = -\frac{T_i}{\lambda_n}(-1)^n \tag{5}$$

and

$$\lambda_n = \frac{n\pi}{R} \tag{6}$$

R being the radius of the spherical droplet.

The idea of the first order approximation is that the A_n coefficients of the solution series in Equation 4 are decreasing with increasing n, in fact the first term is dominating in most cases. Thus, neglecting the terms for $n > 1$, from Equation 4 one can compute the time needed to freeze the droplet as:

$$ft = -\frac{1}{\lambda_1^2 \alpha} ln\left(\frac{\theta_c r_c \lambda_1}{\theta_i sin(\lambda_1 r_c)}\right) \quad (7)$$

$\theta_c = T_f - T_e$ is the critical temperature difference for freezing, r_c is the smallest radius we require to freeze (assuming that the front propagates from the exterior), $r_c = 0.1R$ should be sufficient for most cases.

4. RESULTS

Due to the inherent difficulties in carrying out ice accretion experiments, there is relatively little experimental data available in the literature reporting ice accretion results in well controlled conditions. We chose to apply the glaze ice model on three sets of data, Cases 1 and 3 from Hochart et al. [18] and Run 308 from Wright et al. [19].

4.1. Comparison to the data from Hochart et al. [18]

4.1.1. Case set up

In Hochart et al [18] ice accretion on a NACA 63415 airfoil is investigated in glaze and rime ice conditions. Cases 1 and 3 from [18] correspond to mild and severe glaze ice conditions, respectively. The details of the experimental conditions as well as the amount of accreted ice measured in the experiments are summarised in Table 1.

Table 1. Summary of the experimental cases [18]

Parameter	Case 1	Case 3
LWC $[g/m^3]$	0.37	0.48
MVD $[\mu m]$	27.6	27.6
T_e $[^oC]$	-1.4	-1.4
$\underline{u}_{\text{rel}}$ $[m/s]$	19.9	56.0
t [min]	14.8	24.8
α $[^o]$	6	6
average accreted ice $[g]$	48	354
standard deviation $[g]$	0.25	4.5

The parameter choices and the resulting amount of accreted ice for the computed cases are shown in Table 2. The predictions for Case 1 used 12 loops and a scaling factor of $f = 1000$ to predict the amount of accreted ice. Thus, each iteration in the loop computed the ice accretion for 0.074 s physical time and the airfoil surface was adjusted by assuming that the same trend is valid for 74 s. Since Case 3 involves more severe icing, the number of loops was increased to 25 (each iteration corresponds to 0.062 s), the scaling factor being the same as in Case 1.

A general observation is that the computations are consistently over-predicting the amount of accreted ice, the error being significantly larger for the case with severe icing condition. Furthermore, the predicted amount of accreted ice does not change significantly with changes in the model parameters.

Table 2. Summary of the computed cases

Case	Case in [18]	ft [s]	e [-]	Accreted ice mass [g]	Error [%]
C1T00	1	0.0	0.0	59.52	24.0
C1T01	1	0.1	0.0	59.40	23.7
C1T10	1	1.0	0.0	59.48	23.9
C1T01E05	1	0.1	0.5	59.32	23.6
C3T00	3	0.0	0.0	559.07	57.9
C3T01E05	3	0.1	0.5	563.05	59.1
C3T01E08	3	0.1	0.8	558.55	57.8

4.1.2. Hochart Case 1

Figure 2 shows the isocolors of the average static pressure at the end of the ice accretion event (14.8 minutes) for Case 1. For visualisation purposes, the instantaneous snapshots of the lagrangian parcel field at the last calculated timestep is shown as well. Note, that the lagrangian field is uniformly down-sampled to improve visibility. Figure 2a shows the results when the model was set up to mimic rime ice conditions (by setting $ft = 0$), whereas Figure 2b displays the results for $ft = 0.1$ s and $e = 0.5$. One can observe the smoother ice shape in the leading edge region. Also the higher density of the parcels impacted on the surface stretches to a larger downstream distance in the glaze ice case compared to rime ice conditions.

The influence of the imposed freezing time is illustrated in Figure 3. The figure shows the contour of the clean airfoil (black) together with ice accreted airfoils by setting the model parameter for the freezing time to 0 s (blue, modelling rime ice conditions), 0.1 s (red) and 1 s (green). As a comparison, the timescale based on the relative velocity and the chord length is 0.01 s. The leading and trailing edge regions are enlarged for better visibility. One can observe that even allowing a relatively long freezing time, the shape of the ice does not change significantly. The reason is that the second model parameter, e, controlling the elasticity of the droplet collision with the surface was set to zero. As a consequence, the impacting droplet parcels were trapped in the low velocity region in the proximity of the wall, leading to very small displacements even for long freezing times.

The influence of the parameter controlling the elasticity of the impact is shown in Figure 4, where the clean airfoil (black) is compared to ice accreted airfoils with the same freezing time (0.1 s) but having $e = 0$ (red, no rebounce) and $e = 0.5$ (orange,

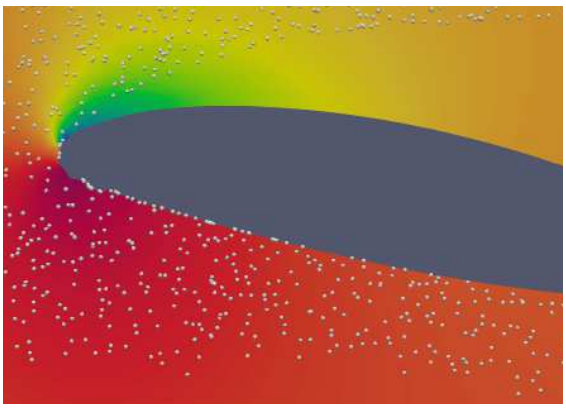

(a) ft=0

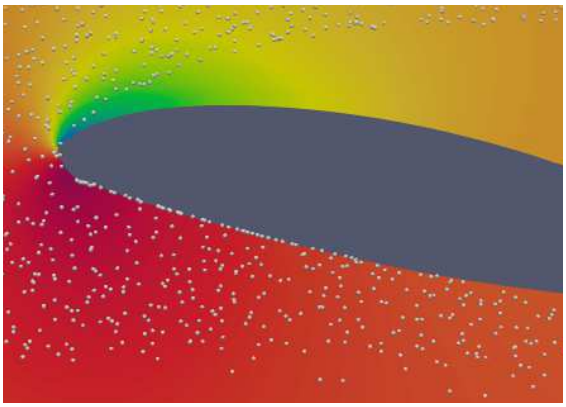

(b) ft=0.1, e=0.5

Figure 2. Illustration of the flow field for Case 1, (a) rime ice model and (b) glaze ice model

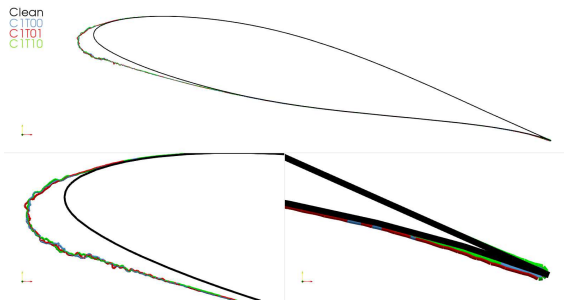

Figure 3. Comparison of the clean and ice accreted airfoil contours for different values of the freezing time. Case 1.

partially elastic collision). One can observe that adjusting the elasticity parameter leads only to minor changes in the accreted ice shape. The quantitative changes are also minor, the error decreases only with 0.1% (see table 2).

4.1.3. Hochart Case 3

Case 3 corresponds to extreme icing conditions and was chosen in order to 'stress-test' the model, to emphasise limitations and clarify targets to be improved in the future.

Figure 5 shows the isocolors of static pressure

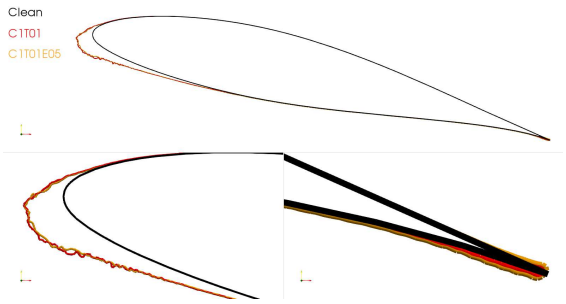

Figure 4. Comparison of the clean and ice accreted airfoil contours for different values of the elasticity parameter. Case 1.

and the droplet parcel field for Case 3 with three different settings of the model parameters. Figure 5a shows rime ice conditions (ft=0), the other two subfigures illustrate glaze ice conditions with different settings of the elasticity parameter.

Unfortunately, all three computations resulted in significant over-prediction of the amount of accreted ice and in the formation of excessively large hornlike structures which are not likely to occur in reality. The closest resemblance to the experimentally observed shapes reported in [18] is found for ft=0.1 s, e=0.5 (Figure 5b): both the tendency to form a shape with two bumps on the suction side and to collect ice in the trailing edge region are captured qualitatively, however, the accreted ice does not have the smooth shape on the pressure side like in the experiments.

4.2. Comparison to the data from Wright et al. [19]

4.2.1. Case set up

Among the multitude of cases reported in [19] the case called Run 308 was chosen since it is a glaze ice case in relatively severe icing conditions. The main parameters describing the icing event are listed in Table 3.

Table 3. Summary of the experimental case [19]

LWC $[g/m^3]$	1.0
MVD $[\mu m]$	20.0
T_e $[K]$	262.04
$\underline{u}_{\text{rel}}$ $[m/s]$	102.8
t [min]	3.85
Airfoil	NACA 0012
α $[^o]$	4

4.2.2. Sample results

Three parameters have been evaluated for this case.

The influence of smoothing of the accreted ice amount is visualised in Figure 6a. Three cases are shown with 1 (red), 10 (green) and 200 (blue) smoothing iterations. As it was expected, smoothing decreases the irregularity of the resulting ice surface. Furthermore, the amount of accreted ice changes as

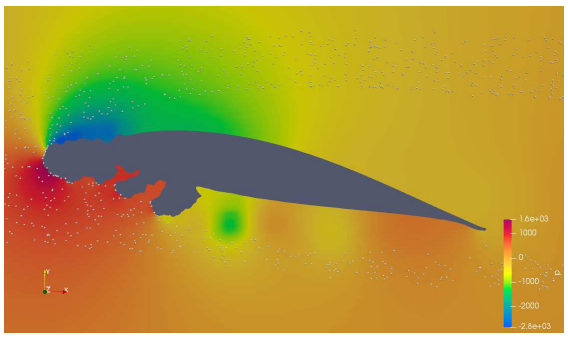

(a) ft=0

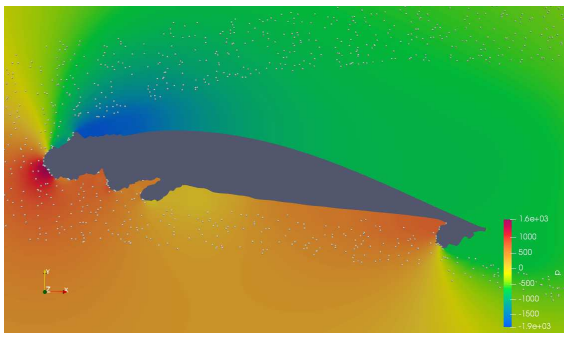

(b) ft=0.1, e=0.5

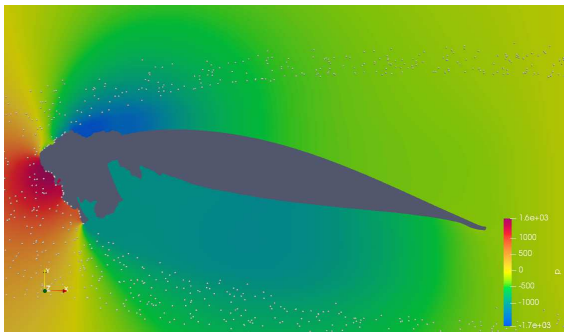

(c) ft=0.1, e=0.8

Figure 5. Illustration of the flow field for Case 3 for three different parameter combinations

well, especially on the pressure side. The reason is that due to smoothing there are smaller irregularities in this region and fewer droplets are collected.

The influence of freezing time is shown in Figure 6b. The rime ice case (ft=0, blue) is compared to glaze model cases with ft=0.1 s and ft=0.2 s. The main impact of the freezing time in this set-up is the reduction of the amount of accreted ice. This is expected since the droplets do not freeze instantaneously. It was expected to see the limit of accreted ice further downstream for glaze conditions. Nevertheless, such effect cannot be observed, probably due to the shape of the accreted ice in the leading edge region.

Finally, the influence of the elasticity parameter, e, is shown in Figure 6c. As it can be seen, with the decrease of e fewer droplets accrete on the surface, the $e = 0.9$ case being very close to the results obtained in rime ice conditions.

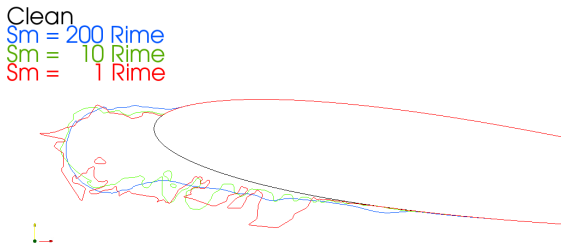

(a) Smoothing

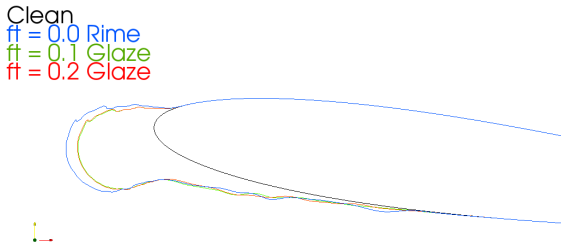

(b) ft

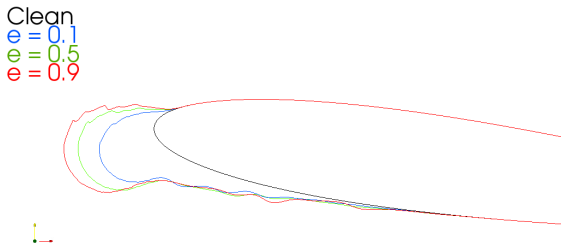

(c) e

Figure 6. Influence of the model parameters on the accreted ice shape.

5. SUMMARY

This work has been a first attempt to implement a fast ice accretion model applicable for glaze ice conditions. Considering the fact that the amount of physical models is significantly reduced we deem that the accuracy of the model is reasonable for mild icing conditions. For severe icing conditions; however, the error in the predicted ice mass increases significantly and unexpected ice shapes are formed, thus further model improvements are needed.

Both the overprediction of the amount of ice and the shape of the ice structures indicate that one significant deficiency of the model is that it does not account for ice loss due to shedding. In reality, ice horns might break due to the aerodynamic forces acting on them. Thus, an important improvement of the model would be to account for ice loss, that feature being important both for rime and glaze ice conditions. We expect that by allowing ice loss both the amount of accreted ice and it's shape would be closer to the experimentally observed ones. By removing the protruding ice horns, fewer droplet parcels would

be captured in the leading edge region and more parcels are expected to deposit further downstream on the pressure side, as it was observed in the experiments.

The model parameters have been adjusted in an ad-hoc manner so far. However, when more experimental data will be available, we expect that the model parameters could be more systematically validated and correlations between icing conditions and the model parameters can be found.

ACKNOWLEDGEMENTS

Financial support for this work was provided by the Swedish Energy Agency, project no. 47053-1. The computational resources were provided by the Swedish National Infrastructure for Computing (SNIC), partially funded by the Swedish Research Council through grant agreement no. 2018-05973 and by LUNARC.

REFERENCES

[1] Stoyanov, D. B., and Nixon, J. D., 2020, "Alternative Operational Strategies for Wind Turbines in Cold Climates", *Renewable Energy*, Vol. 145, pp. 2694–2706.

[2] Badman, D., and Tengblad, Y., 2021, "Roadmap 2040Wind Power: Combating Climate Change and Improving Competitiveness", *Tech. rep.*, Swedish Wind Energy Association.

[3] Laakso, T., Baring-Gould, I., Durstewitz, M., Horbaty, R., Lacroix, A., Peltola, E., Ronsten, G., Tallhaug, L., and Wallenius, T., 2010, "State-of-the-art of wind energy in cold climates".

[4] Jones, R., and Williams, D., 1936, "The Effect of Surface Roughness of the Characteristics of the Airfoils NACA 0012 and RAF 34", *Tech. Rep. Report No.1708*, British ARC.

[5] Gulick, B., 1938, "Effect of Simulated Iced Formation on the Aerodynamic Characteristics of an Airfoil", *Tech. Rep. R.N. NACA- Wr.L-292*, NACA.

[6] Makkonen, L., 1985, "Heat transfer and icing of a rough cylinder", *Cold Regions Science and Technology*, Vol. 10, pp. 105–116.

[7] Makkonen, L., 2000, "Models for the growth of rime, glaze, icicles and wet snow on structures", *Philosophical Transactions of the Royal Society A: Mathematical, Physical and Engineering Sciences*, Vol. 358 (1776), pp. 2913–2939.

[8] Wright, W., 2008, "User ' s Manual for LEWICE Version 3 . 2", *Tech. Rep. NASA/CR–2008-214255*, NASA.

[9] Homola, M. C., Virk, M. S., Wallenius, T., Nicklasson, P. J., and Sundsbø, P. A., 2010, "Effect of atmospheric temperature and droplet size variation on ice accretion of wind turbine blades", *Journal of Wind Engineering and Industrial Aerodynamics*, Vol. 98 (12), pp. 724–729.

[10] Gori, G., Zocca, M., Garabelli, M., Guardone, A., and Quaranta, G., 2015, "PoliMIce: A simulation framework for three-dimensional ice accretion", *Applied Mathematics and Computation*, Vol. 267, pp. 96–107.

[11] Jin, J. Y., and Virk, M. S., 2019, "Study of ice accretion and icing effects on aerodynamic characteristics of DU96 wind turbine blade profile", *Cold Regions Science and Technology*, Vol. 160 (September 2018), pp. 119–127.

[12] Prince Raj, L., Yee, K., and Myong, R., 2020, "Sensitivity of ice accretion and aerodynamic performance degradation to critical physical and modeling parameters affecting airfoil icing", *Aerospace Science and Technology*, Vol. 98, p. 105659.

[13] Szasz, R., and Fuchs, L., 2012, "Numerical modeling of ice accretion on a wing section", J. Vad (ed.), *Proceedings of the Conference on Modelling Fluid Flow*, pp. 292–298.

[14] Szasz, R.-Z., Ronnfors, M., and Revstedt, J., 2016, "Influence of ice accretion on the noise generated by an airfoil section", *International Journal of Heat and Fluid Flow*, Vol. 62, pp. 83–92.

[15] Son, C., and Kim, T., 2020, "Development of an icing simulation code for rotating wind turbines", *Journal of Wind Engineering and Industrial Aerodynamics*, Vol. 203 (June), p. 104239.

[16] "OpenFOAM, https://www.openfoam.org".

[17] Menter, F., 1994, "Two-Equation Eddy-Viscosity Turbulence Models for Engineering Applications", *AIAA Journal*, Vol. 32, pp. 1598–1605.

[18] Hochart, C., Fortin, G., Perron, J., and Ilinca, A., 2008, "Wind turbine performance under icing conditions", *Wind Energy*, Vol. 11 (4), pp. 319–333.

[19] Wright, W. B., and Rutkowski, A., 1999, "Validation Results for LEWICE 2.0", *Tech. rep.*, Lewis Research Center.